APPENDIX A: FABRIC CHARACTERIZATION

The objective of the current research was to incorporate experimentally determined in-plane shearing, tensile, bending stiffness, and friction information of the composite fabrics used in the production of a wind turbine blade into a finite element model. The model should be capable of capturing the deformation of the yarns during fabric layup (by hand or automated layup) as well as during the vacuum compaction stage of the manufacturing process, thus giving insight as to areas where defects may be developed. Subsequently, by knowing how the yarns have deformed during these two stages, the structural stiffness of the blade can be predicted with fewer assumptions and without knockdown factors, thereby linking the resulting composite structure to the manufacturing process. These structural models can then predict the effect of defects on various blade sizes and in different locations within the blade. This simulation of the manufacturing process and subsequent structural stiffness can help guide design decisions such as the number of layers and orientations required for a given selection of fabric(s) that will reduce weight while maximizing structural performance. The credibility of these simulations is dependent upon an experimental characterization of the dry fabric material as well as the cured composite architecture.

The mechanical behaviors of the six NCFs used in the blade design were experimentally characterized and then implemented into a model of the blade in Abaqus/Explicit. The fabrics used in this study are manufactured by Vectorply Corporation®. Properties of the fabrics and the resin are provided in Tables A-1 and A-

2, respectively. This appendix describes the experiments conducted to characterize the mechanical behavior of the non-crimp fabrics for implementation into the model.

Table A-1. Properties of various fabrics studied

Manufacturer's style	Fiber Type	Architecture	Area Density (g/m^2)	Thickness (mm)
E-LT 5500	E-Glass	$0^o/90^o$ Biaxial	1842	1.45
E-LT 2900	E-Glass	$0^o/90^o$ Biaxial	978	0.91
E-BXM 1708	E-Glass	$45^o/-45^o$ Double Bias w/Chopped Fiber Mat	882	1.17
E-BXM 1208	E-Glass	$45^o/-45^o$ Double Bias w/Chopped Fiber Mat	700	0.91
E-BX 0900	E-Glass	$45^o/-45^o$ Double Bias	334	0.31
C-LA 2012	Carbon	0^o Unidirectional	710	1.12

Table A-2. Properties of HEXION RIMR 135 Epoxy at room temperature

Density (g/cm^3)	1.18-1.20
Viscosity (mPas)	700-1100
Flexural Strength (MPa)	90-120
Modulus of Elasticity (MPa)	2700-3200
Tensile Strength (MPa)	60-75
Compressive Strength (MPa)	80-90
Elongation of Break (%)	8-16
Impact Strength (kJ/m^2)	70-80

1 DRY FABRIC MODELING

The discrete approach in the current research utilized a commercially available finite element package (Abaqus), where standard beam and shell elements were used in conjunction with a user-defined material subroutine to model the fabric blanks using a hypoelastic description. The use of these common element types allows a similar approach to be extended to other popular finite element packages with user material subroutine capabilities such as LS-DYNA and ANSYS, without the need for any special-purpose element types. Such an approach is attractive to industry because the method uses commercially available finite element codes.

The unit cell of a biaxial non-crimp fabric composite is illustrated in Figure A-1 [1], and consists of four 1-D beam elements merged to the perimeter of a 2-D shell. The 2-D shell element defines the fabric shear stiffness, and the beam elements simulate the yarns of a fabric and capture the tensile and bending stiffnesses of the fabric. The effect of the through stitching is captured by the pin-jointed connections at the nodes.

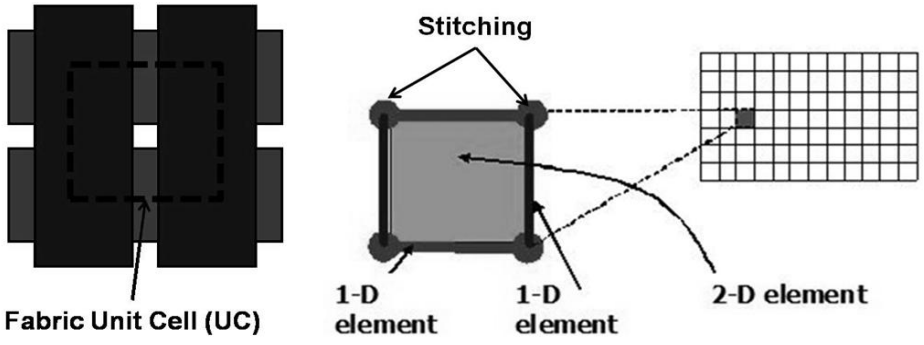

Figure A-1. Principle of the discrete mesoscopic modeling using a combination of 1-D and 2-D elements [1]

Regressions of experimental data were used to conclude empirical models that were then implemented as user-defined material subroutines to capture the mechanical behavior of the fabric material in the finite element solver [2]. Finite element models of the various tests were completed to validate that the fabric model behavior can be properly simulated using the finite element method. Additionally, the finite element method allows for contact to be defined between layers of fabric [3].

2 FABRIC ARCHITECTURE

Table A-1 summarized the six non-crimp fabrics used in the manufacture of the 9-meter CX-100 wind turbine blade.

The biaxial fabrics, E-LT 5500 and E-LT 2900, consist of thick 0^o yarns on one side (Figure A-2a) and much thinner 90^o yarns on the other side (Figure A-2b). The 0^o and 90^o yarns are held together by a through-thickness stitching oriented along the 0^o yarns. As indicated in Table A-1, the E-LT 5500 has a greater areal density and thickness when compared to the E-LT 2900. The spacing of the stitching (unit-cell width) is also slightly greater in the E-LT 5500. These biaxial fabrics are primarily used in the root section of the CX-100 wind turbine blade.

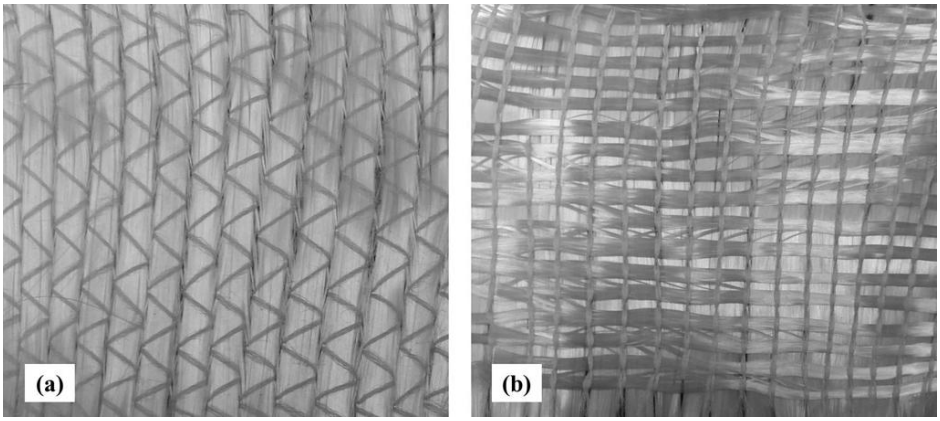

Figure A-2. Biaxial NCF architecture

The double-bias fabrics, E-BXM 1708, E-BXM 1208, and E-BX 0900, consist of $+45^{o}$ and -45^{o} layers of the same-size yarns (Figure A-3a). The stitching in these fabrics is oriented in the 0^{o} direction. The architecture of each of these three fabrics is the same, but the areal densities and thicknesses of each fabric differ, as indicated by Table A-1. In addition, the E-BXM 1708 and E-BXM 1208 include a mat of random chopped glass fibers on one side (Figure A-3b). This mat facilitates the soaking of the resin during the resin infusion process and does not otherwise affect the mechanical behavior of the dry fabric. The double-bias fabrics cover most of the CX-100 skin area.

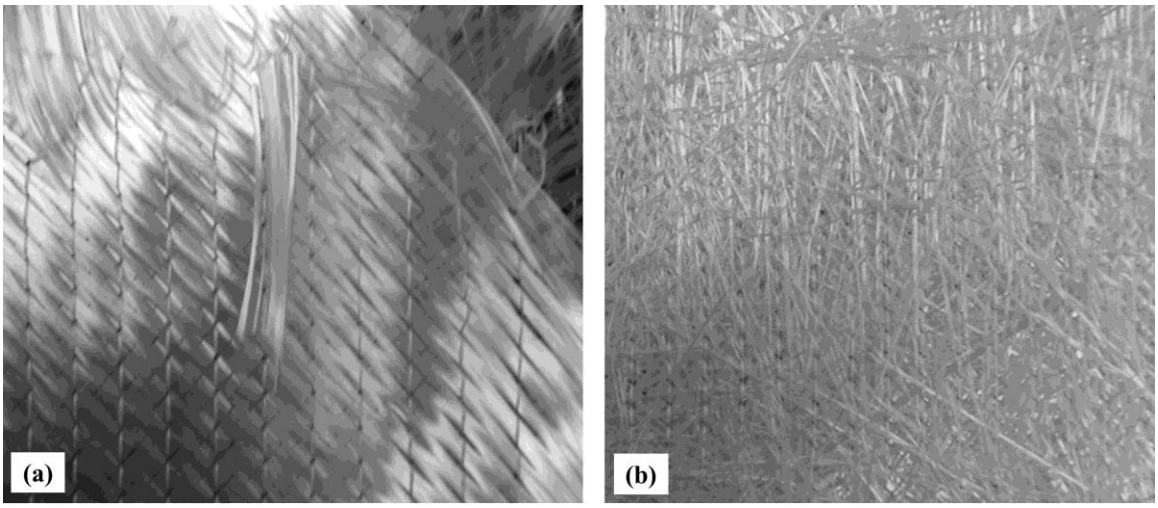

Figure A-3. Double-bias NCF architecture showing (a) ± 45^{o} yarns and (b) random chopped fiber mat

Finally, the carbon unidirectional fabric, C-LA 2012, is used in conjunction with the E-BX 0900 double-bias fabric to form the spar cap. The architecture of this fabric (Figure A-4) is similar to that of the biaxial fabrics, only without the 90^{o} yarns.

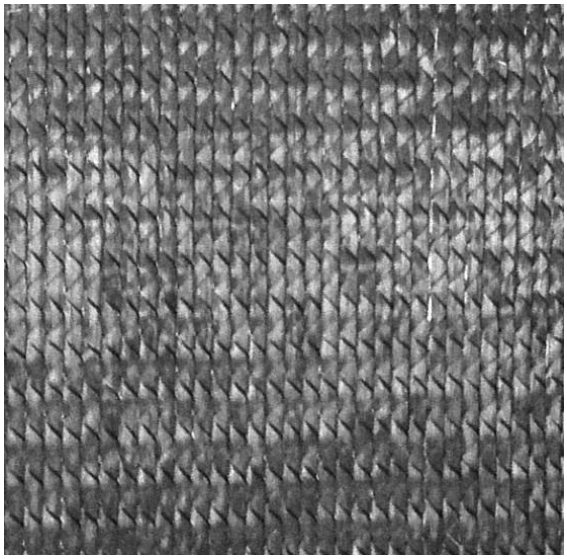

Figure A-4. Unidirectional carbon NCF architecture

4. MATERIAL TESTING

The shear, tensile and bending mechanical behaviors of the fabrics are characterized using a standardized set of tests.

4.1 SHEAR-FRAME TESTING

The standard test for measuring the shear behavior of fabrics is the shear-frame test [4], also known as the trellis-frame test, or the picture frame test, as shown in Figure A-5. In this test, a fabric specimen is clamped with the yarns typically directed perpendicular and parallel to the four clamping bars. Shear deformation is developed by fixing one corner and applying a tensile load on the opposing corner. The shear-frame test assumes that the shear angle is uniform over the entire sample and equal to the frame angle. These two assumptions have been verified for woven fabrics via Digital Image Correlation (DIC) [5, 6]. The deformation of the fabric in the shear-frame test is shown in Figure A-6. For this research, a minimum of three samples was tested for each fabric.

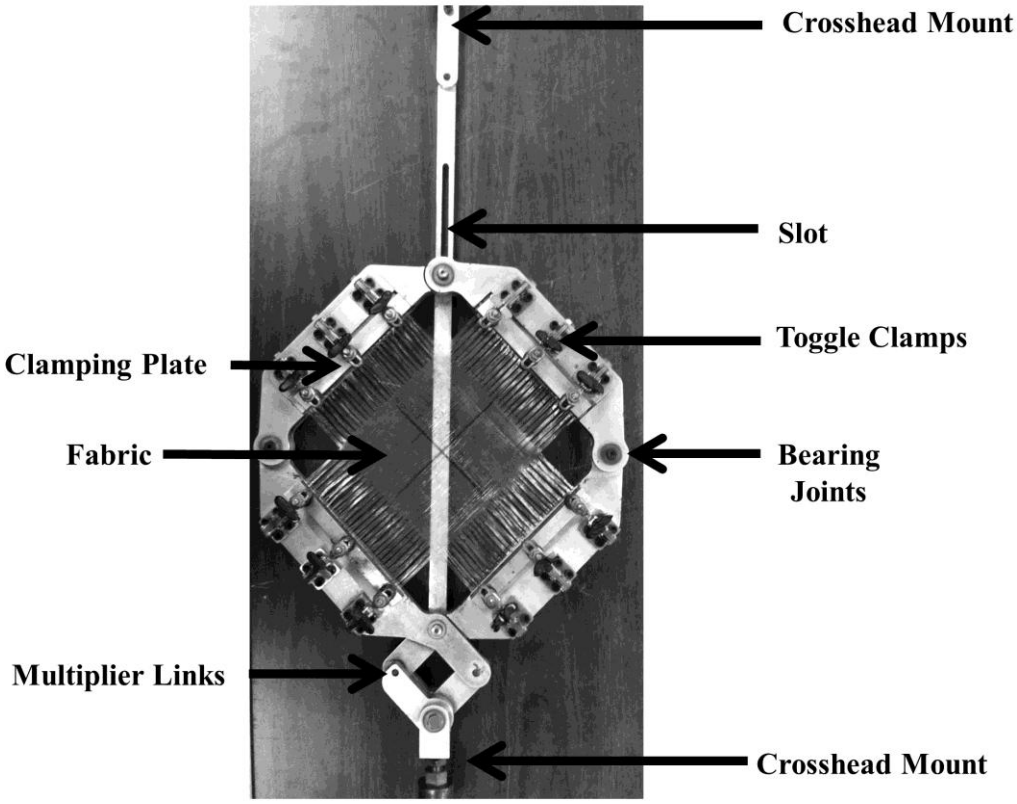

Figure A-5. Shear-frame test

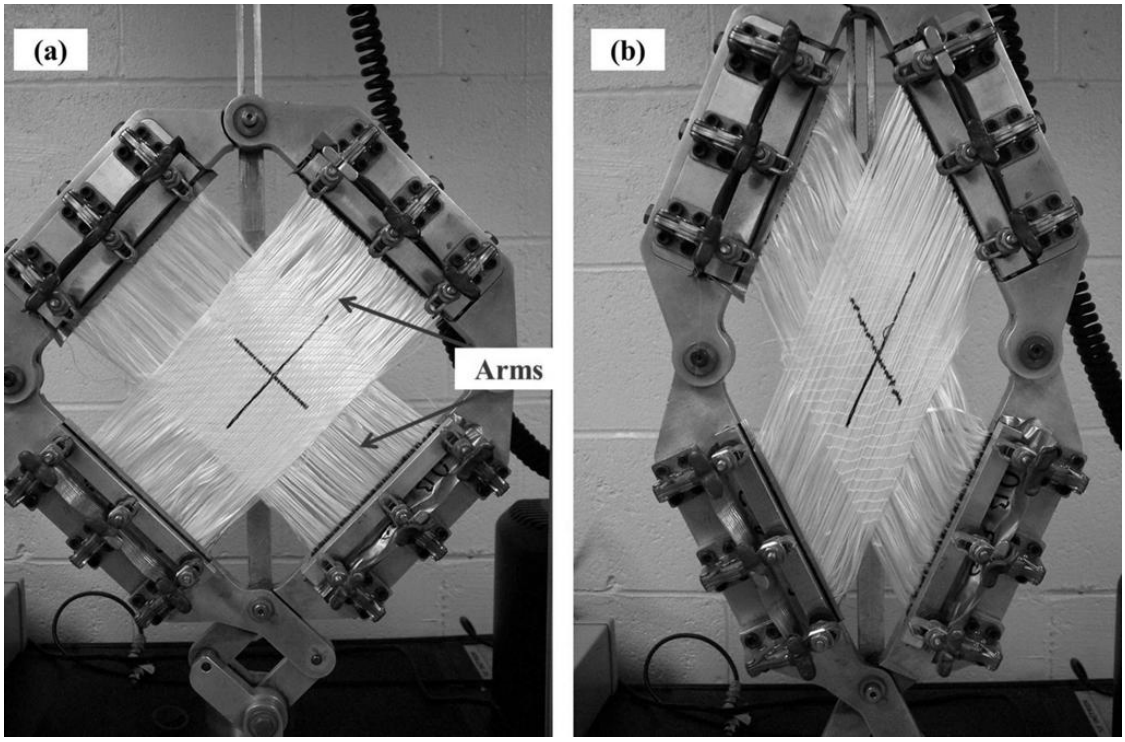

Figure A-6. Deformation of shear-frame test (a) before deformation and (b) after deformation

The cross yarns are removed in the arms of each sample to minimize edge effects and allow the yarns to rotate freely relative to each other. Consider the unidirectional carbon fabric, C-LA 2012. This fabric is mounted in the shear frame in only one direction, because there are no perpendicular yarns. Without the presence of "arms" in the sample, an out-of-plane wave pattern is observed across the width of the test sample and extending along its whole length when pulled in the frame (Figure A-7a). The out-of-plane deformations are caused by the clamped fabric edges, which do not allow individual fibers to slide relative to each other. The stitching between the yarns was partially cut to create 50-mm arms at each end of the sample (Figure A-7b). The addition of arms allowed for in-plane sliding of the yarns in the middle of the sample, as shown in Figure A-7c, and significantly reduced out-of-plane deformation [7].

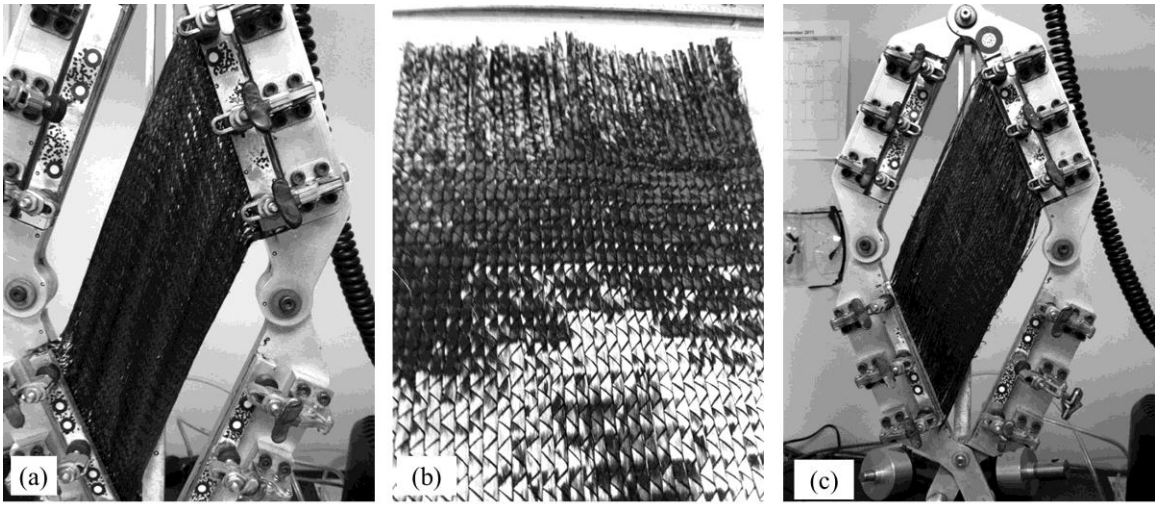

Figure A-7. Unidirectional NCF loaded in the shear frame (a) without arms. The absence of arms causes out-of-plane deformation due to edge effects, which necessitates the (b) addition of arms in the sample. The arms (c) significantly reduce the out-of-plane deformation

Woven fabric samples are typically loaded and unloaded several times in the shear frame before measuring the shear stiffness. The intent of this mechanical conditioning is to reduce the effect of undesired tension in the yarns that could arise from a misalignment of the yarns [4, 8]. The mechanical conditioning also allows for increased repeatability from sample to sample even though in reality, a fabric will be taken off of a roll and laid into a mold without any mechanical conditioning. Typically for a given sample, the measured loads during the first shear-frame test run will be higher than those of the subsequent runs, in which the load curves appear to be very similar. Non-crimp fabrics, however, are more sensitive to mechanical conditioning because of the through-thickness stitching which can tear after repeated loading and unloading of the same sample. This stitching plays a very important role in the shear stiffness and in the wrinkling characteristics of a NCF and cannot be neglected. Therefore, for the fabrics

studied in this research, the samples were not mechanically conditioned, and the first load-displacement curve was taken as the representative shear deformation curve.

The measured load is converted to a force that is normalized by the length of the frame. This normalization accounts for various shear-frame sizes and allows for comparison between labs with differing frame sizes. The normalized force can then be divided by the thickness of the fabric sample to obtain the shear stress. Similarly, the shear angle can be determined by knowing the length of the frame, length of the fabric sample, and the measured displacement data. This angle can then be converted to a logarithmic shear strain, which is consistent with the shear strain definition used by the finite element code. After testing a minimum of three samples, the average shear stress and logarithmic strain are calculated and plotted with error bars of one standard deviation.

After all of the stress-logarithmic strain plots have been generated, polynomial fits are made to these curves. These functions are implemented into Abaqus/Explicit via its user-defined material subroutine, VUMAT, to capture the shear behavior of each fabric. Abaqus/Explicit uses rate-independent constitutive equations, also called hypoelastic laws, to model large deformation and strains. Stresses are updated using:

$$\sigma_{ij}^{t+1} = \sigma_{ij}^{t} + \Delta\sigma_{ij}^{t+1} \tag{1}$$

$$\Delta\sigma_{ij}^{t+1} = C_{ijkl}.\Delta\varepsilon_{kl}^{t+1/2} \tag{2}$$

where $\Delta\sigma_{ij}^{t+1}$ is the stress increment at time step t+1, C_{ijkl} is the constitutive matrix and $\Delta\varepsilon_{kl}^{t+½}$ is the midpoint strain increment obtained from the integration of the strain rate tensor. The custom constitutive models obtained through regressions of experimental

data and implemented into the VUMAT subroutine are linked with the overall solver to update the stress (Equation 2). The strain increment, $\Delta\varepsilon_{kl}^{t+½}$, is given by the solver to VUMAT that subsequently returns the corresponding stress increment to the solver. The stress update is made in the local reference frame for the element, i.e. a co-rotational frame that rotates with the element. The summation of the strain increments gives a logarithmic (or true) strain in the principal-stretch directions. Details associated with the constitutive equations as they pertain to the 1-D and 2-D elements of the current unit-cell model are provided in [2]. The VUMAT subroutine is provided in Appendix A.

A finite element model of the fabric shear-frame test, including the "arms" of the specimens, is generated to ensure that the 2-D shell elements are accurately capturing the shear stiffness of each fabric (Figure A-8a). The arms are modeled using 1-D beam elements, and the frame is modeled using four aluminum trusses with a cross section of 500 mm^2. The constants that define the tangent shear modulus are obtained by deriving the polynomial fits of the experimental stress-logarithmic strain curves and are defined in the Abaqus input file material card. The model correlates with the assumption of pure shear in the fabric sample (Figure A-8b).

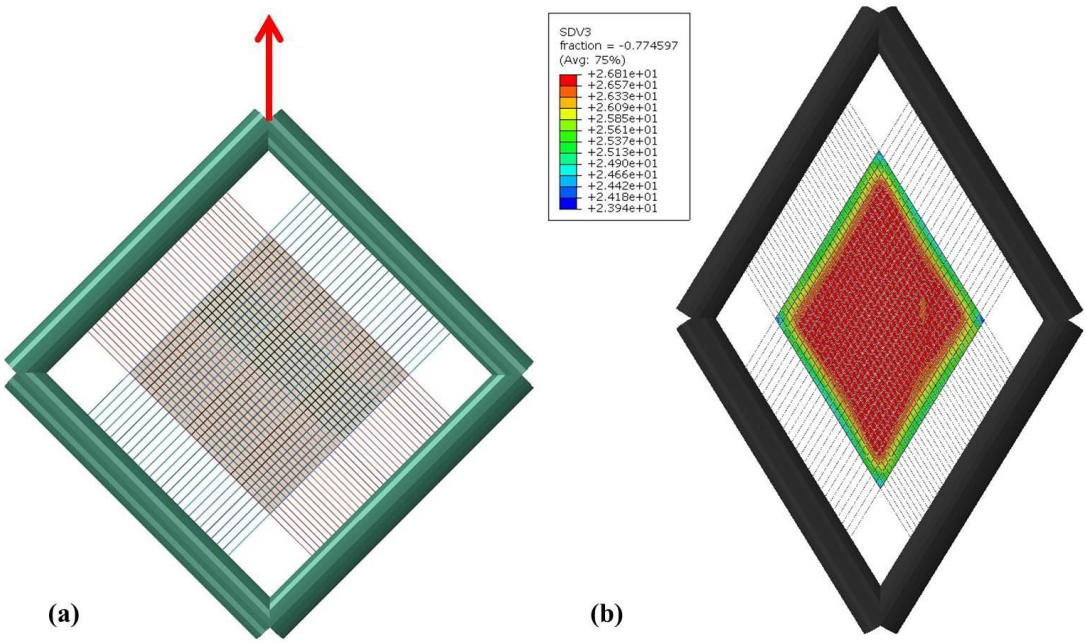

Figure A-8. Finite element model (a) of the shear-frame test and (b) the resulting uniform shear angle contours

4.2 Tensile testing

As fabric is pressed into a mold, certain yarns may exhibit high tensile stresses as they bridge undulated regions of the geometry, i.e. peaks and valleys. These high tensile stresses can ultimately cause the yarns to break, leading to a poor-quality part. While the current material model does not allow the yarns to visually break, high stresses can be used to indicate local areas where fiber breakage could be a problem. Therefore, to characterize the tensile mechanical behavior of the yarns, uniaxial tensile tests are performed on individual yarns extracted from each fabric.

A minimum of three samples is tested and the gage length is set to 150 mm to ensure that all of the fibers within each yarn are continuous and loaded simultaneously. With longer yarn samples, the measured stiffness is much lower than expected. It is believed that variations in the length of individual fibers result in only a portion of the

yarn being loaded. To prevent slipping at the pneumatic grips (Figure A-9a), tabs are created by consolidating small pieces of Twintex® commingled glass/polypropylene woven-fabric (Figure A-9b). For this research, the crosshead pulled the yarns at a rate of 5 mm/min.

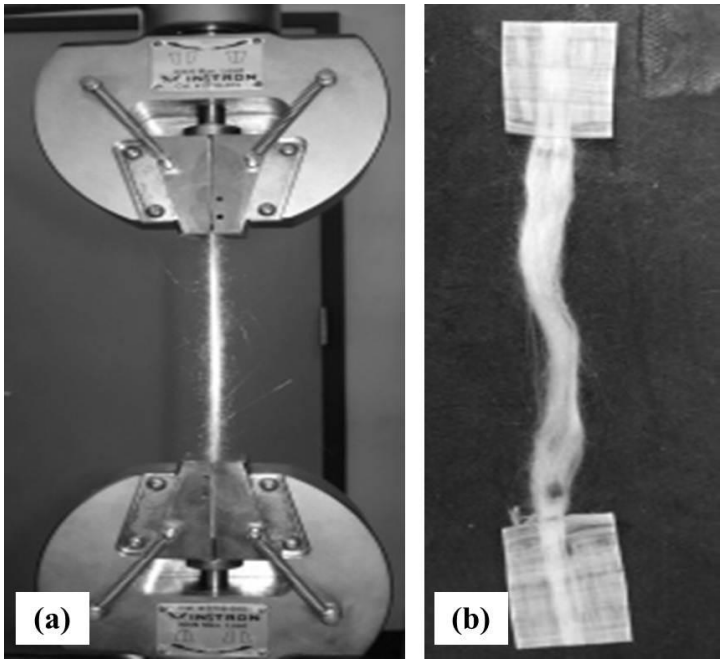

Figure A-9. Tensile test setup with (a) pneumatic grips and (b) Twintex® tabs to prevent yarn slippage

The tensile tests quantify the fracture load (Figure A-10a) and modulus of the yarn. The modulus of each yarn is obtained from the slope of the associated stress/true-strain curve (Figure A-10b), where the stress is determined by dividing the measured load by the effective cross section of the yarn, A_{eff}. This effective cross section of the yarn is determined based on the linear density of the yarn ρ_{linear} and the fiber material density ρ_{mat}:

$$A_{eff} = \frac{\rho_{linear}}{\rho_{mat}} \tag{3}$$

The true strain is used to again be consistent with the finite element code:

$$\varepsilon = \ln\left(1 + \frac{l}{l_o}\right) \tag{4}$$

where l is the measured length of the sample and l_o is the initial length.

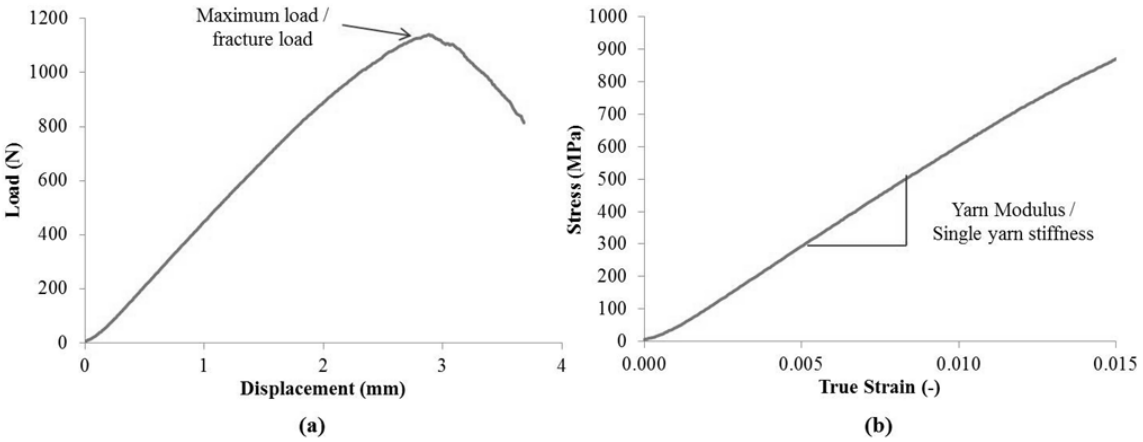

Figure A-10. Yarn tensile testing resulting in (a) a typical load-displacement curve and (b) the determination of the tensile behavior from the modulus for a typical yarn

The individual yarn stress-true strain curves are averaged and plotted with error bars of one standard deviation. Abaqus applies Equation 2 to the definition of the 1-D beam element material behavior, where C_{ijkl} is the tangent tensile modulus, or yarn modulus. A single yarn is modeled using a set of beam elements and pulled uniaxially. The slope of the stress-true strain curve is determined from the model and is compared to the yarn modulus obtained experimentally to ensure that the tensile stiffness is being accurately captured in the finite element fabric model.

4.3 Bending stiffness test

To use the finite element method for predicting the formation of in-plane and/or out-of-plane waviness during the manufacture of composite wind turbine blades, the overall mechanical behavior of the composite fabric reinforcements must be thoroughly defined. The in-plane shearing behavior is often used as an indicator via the "locking angle" as to when wrinkles may develop in the form of in-plane and/or out-of-plane waves. As yarns rotate relative to one another, they eventually reach a point where they can no longer rotate in-plane and must buckle out-of-plane. However, it has been shown that simply relating wrinkling to the shear angle is not sufficient. The formation of wrinkles and/or waves depends on the combination of in-plane shear, tension and bending behaviors of the fabric [9]. Thus, it is important to characterize the bending stiffness of the dry non-crimp fabrics.

When characterizing the dry fabric bending stiffness, a cantilever "beam" method is often used [10], where the fabric is allowed to bend due to its own weight (Figure A-11a). However, depending on the length of the sample, the effective direction of the distributed load on the sample changes due to the large deformations, and thus, a single value for the fabric bending stiffness cannot be concluded for all lengths despite efforts to compensate for the effect of gravity. An alternate method for characterizing the bending stiffness is to align the length of the beam with gravity and thereby reduce the nonlinear loading effects [11]. Fabric samples are clamped at one end and hung vertically. A horizontal load is applied to displace the tip of the fabric a known amount. This load is applied by attaching masses to a string tied to the tip of the fabric sample (Figure A-11b).

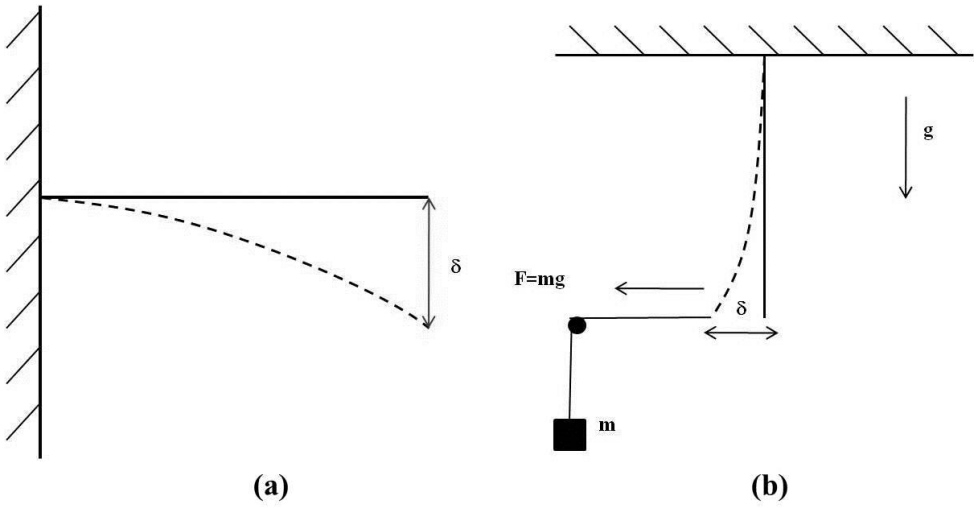

Figure A-11. Schematic of (a) cantilever experimental setup and (b) hanging-fabric bending stiffness setup

With the effective fabric length positioned in the clamp, various tip displacements are applied using an appropriate load, and a digital image of the fabric is captured. Individual data points are generated along the fabric length (Figure A-12a) and plotted (Figure A-12b). At least two different samples of each fabric are tested for repeatability.

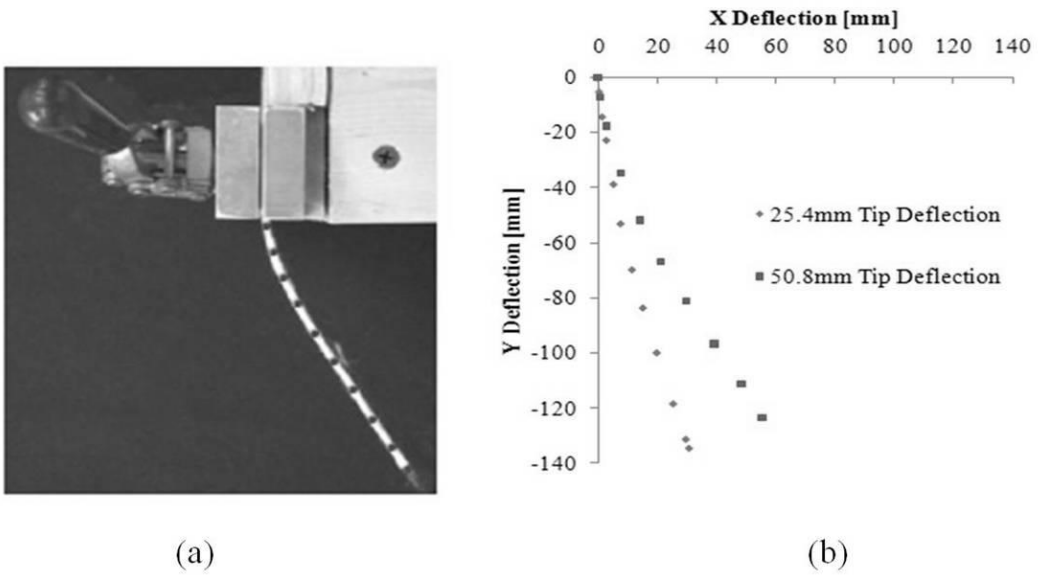

Figure A-12. Postprocessing of experimental data including (a) generation of x and y data points and (b) plotting of data points

Finite element models similar to the experimental fabric samples are used to calibrate the fabric bending stiffness. The bending stiffness is defined per yarn and is therefore assigned to each of the 1-D beam elements in the fabric. Equivalent tip displacements are prescribed in the models, and a range of bending-stiffness values are used to replicate the experimental profile shape of the sample. While several values of bending stiffness may lead to a similar profile shape, the force required to displace the tip a known amount is compared to the experimental force to ensure that the correct bending stiffness is being used in the model. Note that for the effective bending stiffness as used here the unit for moment, M, is N-mm and for curvature, κ, is mm^{-1}. Thus, the bending stiffness M/κ defined in the finite element model is given as $N\text{-}mm^2$. As a means of verifying that the bending stiffness is valid, the bending stiffness is applied to models with different tip displacements and different fabric sample lengths (Figure A-13).

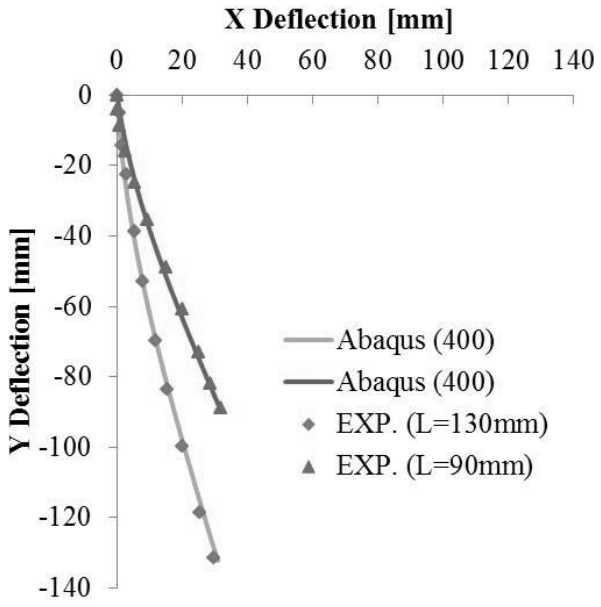

Figure A-13. Comparison of experimental data to FE model of E-LT 5500 NCF for varying tip displacements and fabric lengths

As mentioned previously, the formation of wrinkles and/or waves depends on the combination of in-plane shear, tension and bending behaviors of the fabric. It is certainly possible to predict defects based on the in-plane shear and tension behaviors alone. However, the bending stiffness is needed to describe the wrinkle/wave shape. For example, compressing a fabric sample model from two sides will yield a different number of out-of-plane waves with different amplitudes depending on the magnitude of the bending stiffness. A much stiffer fabric will result in fewer waves with greater amplitude (Figure A-14a) than a fabric with a low bending stiffness (Figure A-14b).

Figure A-14. FE model of a fabric sample compressed from each side with (a) high bending stiffness and with (b) low bending stiffness

In the current unit-cell modeling approach, the 1-D beam elements carry the bending stiffness of the fabric yarns. Without explicitly defining the bending stiffness as part of the beam section properties, Abaqus will by default consider the product of the elastic modulus, E, and the area moment of inertia, I, of the elements to define the bending stiffness. This default definition is typically much higher than the measured bending stiffness.

5 MATERIAL TEST RESULTS

The results of the material characterization results are summarized in the following sections.

5.1 SHEAR FRAME TEST

The in-plane shearing of the fabric yarns is the principal mode of deformation as a fabric layer conforms to the shape of a double-curvature geometry. This in-plane shearing results in a change of the angle between the initially orthogonal yarns of a biaxial non-crimp fabric. The shear-frame test is used to characterize this in-plane shearing behavior. The measured load-displacement data are converted to stress-logarithmic shear strain to be consistent with the definition of shear strain as used by the finite element code. After testing a minimum of three samples, the average shear stress and logarithmic strain are calculated and plotted with error bars of one standard deviation (Figure A-15).

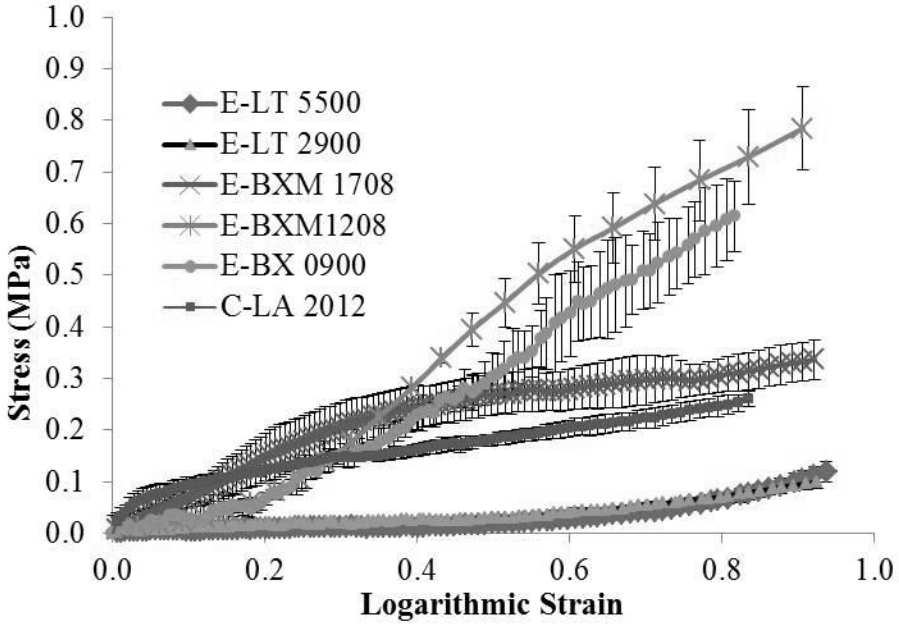

Figure A-15. Shear stress vs. logarithmic strain for various non-crimp fabrics in shear-frame test

In Figure A-15, it can be seen that the stress-strain curve for the carbon unidirectional NCF (C-LA 2012) is similar to the stitched biaxial NCFs (E-LT 5500 and E-LT 2900), but exhibits an overall higher shear stress. The higher stress is most likely due to differences in material, because carbon is much stiffer than glass, as well as due to a tighter stitch pattern in the carbon as compared to the glass fabrics. The tighter stitch pattern in the carbon unidirectional NCF does not allow for as much slipping of the yarns and therefore the adjacent yarns begin to compress against each other much sooner than in the case of the biaxial NCFs. This yarn compaction increases the friction between the yarns and the load subsequently increases.

The stitched biaxial fabrics, E-LT 5500 and E-LT 2900, exhibit behavior very similar to that of woven fabrics (Figure A-16). As shown by a typical load-shear angle curve from the E-LT 5500 in Figure A-17, the yarns are initially orthogonal to one

another. Upon initiation of intra-ply shear deformation, the yarns begin to rotate and possibly to slip relative to one another. The shear stiffness steadily increases as the yarns continue to rotate and compress against each other, thus increasing the friction between adjacent yarns. As the yarns continue to rotate, an angle referred to as the locking angle is reached where the yarns are no longer able to compact easily and the shear stiffness increases rapidly. In addition to a significant increase in stiffness, deformation beyond the locking angle can also cause the fabric to buckle out-of-plane, as the deformation mode becomes a combination of shear, yarn compaction and tension. The locking angle is determined from the intersection of two lines tangent to the load-shear angle curve. This locking angle was determined to be 36^{o} for the biaxial fabrics.

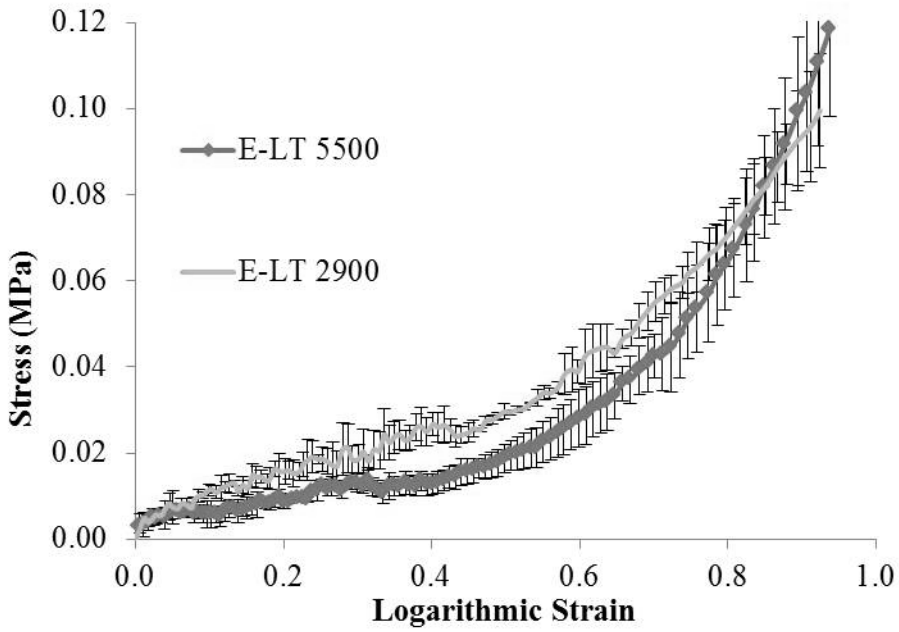

Figure A-16. Shear stress vs. logarithmic strain for biaxial NCFs

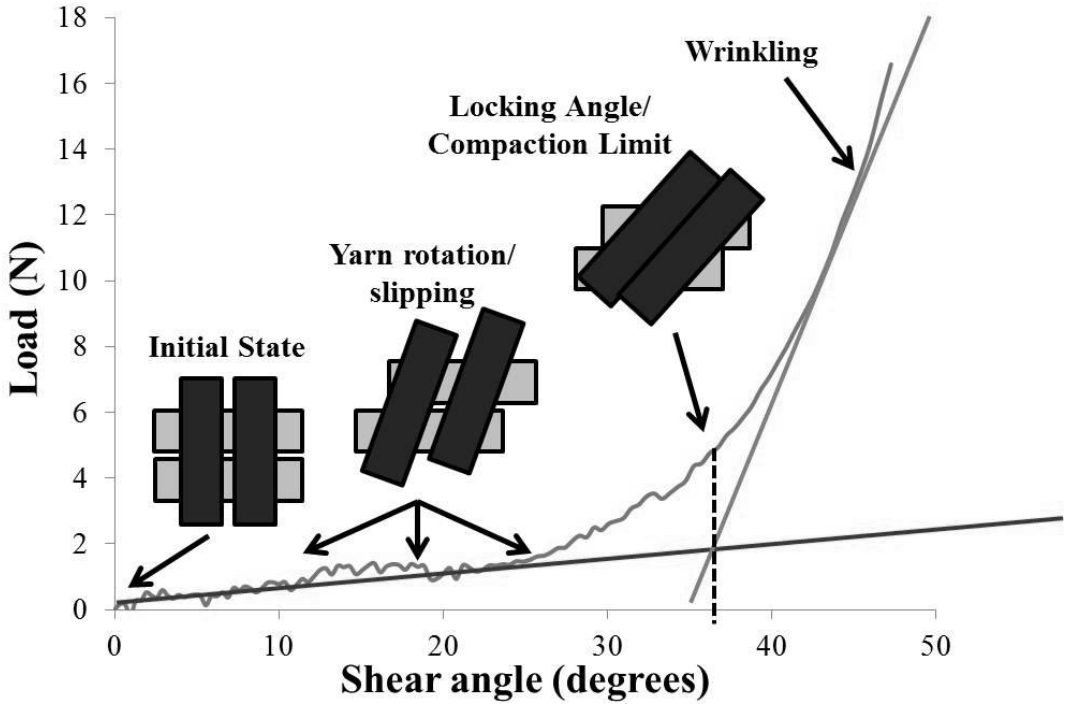

Figure A-17. E-LT 5500 load-shear angle curve with schematics of shear behavior

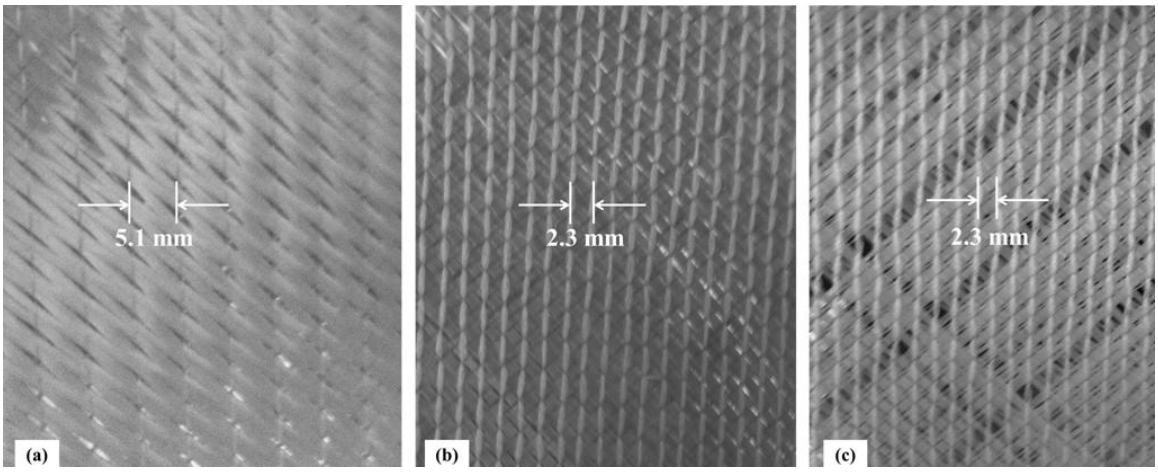

Figure A-18. Stitch pattern in the (a) E-BXM 1708, (b) E-BXM 1208, and (c) E-BX 0900 double-bias NCFs

The orientation of the stitching relative to the ±45^{o} yarns in the double-bias NCFs (E-BXM 1708, E-BXM 1208, and E-BX 0900), as well as the spacing of the stitch

pattern significantly influences the shear behavior of the fabric. Figure A-15 shows that the shear stiffnesses of the double-bias fabrics are much greater than those of the biaxial and unidirectional fabrics. As the sample is loaded in the shear frame, the stitching is subjected to tension which prohibits the yarns from sliding and/or rotating relative to each other. The fabric begins to buckle out of plane very early in the experiment when compared to the biaxial fabric, which begins to show out-of-plane deformation only after exceeding its locking angle. The tighter the stitching pattern, the more vulnerable the fabric will be to buckle out-of-plane. Figure A-18 shows the greater spacing between stitches in the E-BXM 1708 fabric when compared to the E-BXM 1208 and E-BX 0900, results in a lower shear stiffness (Figure A-15). While the stitch pattern is similar between the E-BXM 1208 and E-BX 0900 fabrics, the yarns of the E-BX 0900 are smaller and more spacing is observed between adjacent yarns (Figure A-18c). The increased spacing allows the yarns to slip slightly more than they are able to in the E-BXM 1208 fabric, which explains the slightly lower shear stiffness seen in Figure A-15.

If the fabric is rotated such that the stitching is oriented perpendicular to the loading direction as indicated by the arrow in Figure A-19, the stitching compresses with the sample and therefore allows the yarns to rotate freely relative to each other, much like they do in the case of the biaxial NCF. As a result, very little out-of-plane deformation is observed (Figure A-19b), and the resulting shear stiffness is significantly lower than in the case of the stitching being oriented parallel to the loading direction (Figure A-20).

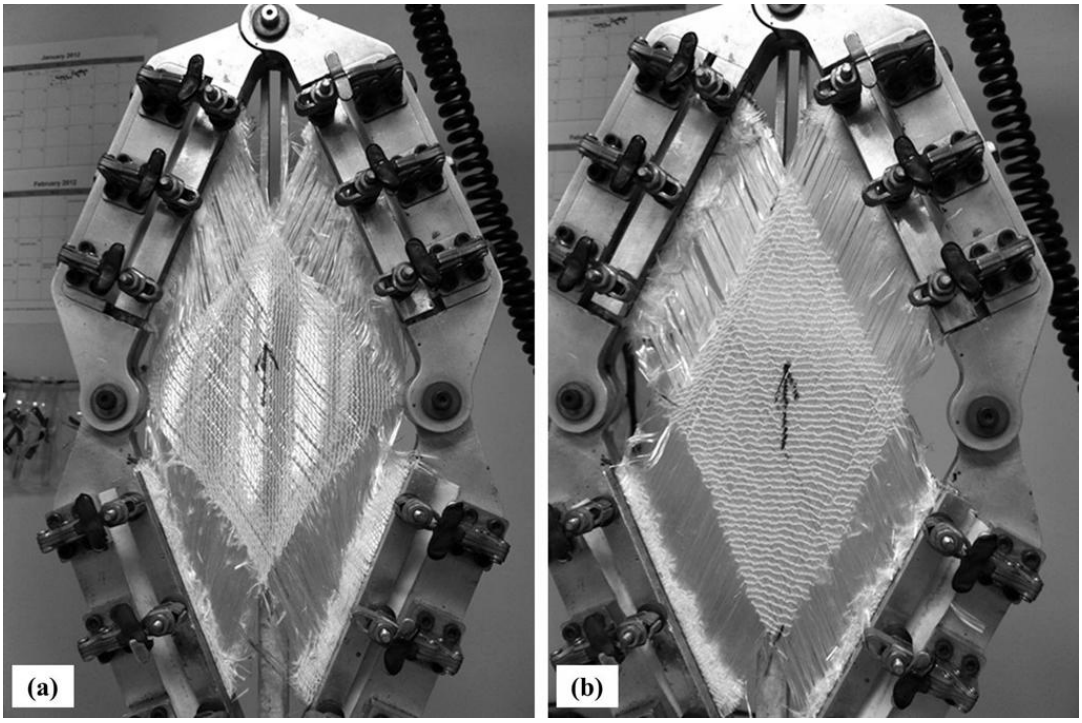

Figure A-19. Double-bias NCF loaded in shear frame with (a) stitching oriented parallel to loading direction and (b) perpendicular to loading direction

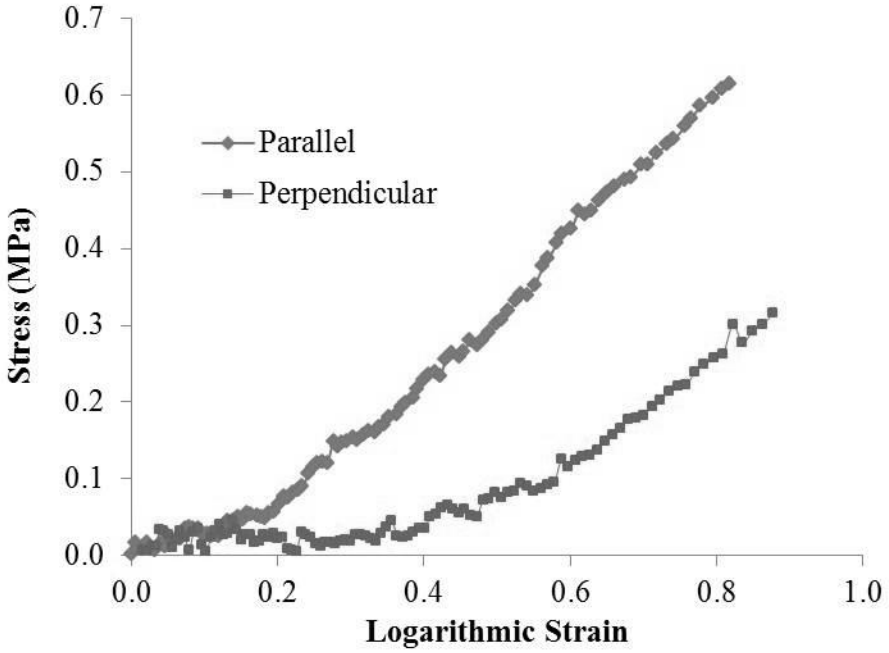

Figure A-20. Effect of through-thickness stitching orientation on shear stiffness of double-bias NCFs. Here, the E-BX 0900 fabric is tested.

Fourth-order polynomial fits of the experimental stress-logarithmic strain curves were used to define the tangent shear modulus, ***D33***, required by the VUMAT material subroutine to define the in-plane shear stiffness of the 2-D shell elements in the finite element model of the fabric. This tangent shear modulus is defined in terms of the logarithmic shear angle, γ_L,

$$D33 = C4|\gamma_L|^4 + C3|\gamma_L|^3 + C2|\gamma_L|^2 + C1|\gamma_L| + C0 \tag{8}$$

where C0, C1, C2, C3 and C4 are the constants defined on the Abaqus material card for each fabric. These constants are summarized in Table A-3 and in Appendix B. Note that Props(1) through Props(5) represent the notation within the VUMAT subroutine for defining the polynomial constants.

Table A-3. Polynomial constants for tangent shear modulus in FE model

Fabric	Props(1)	Props(2)	Props(3)	Props(4)	Props(5)
	C0	C1	C2	C3	C4
E-LT 5500	0.101	-0.825	2.624	-3.234	2.000
E-LT 2900	0.144	-0.858	1.953	-1.041	0.069
E-BXM 1708	0.603	3.192	-19.158	28.600	-13.079
E-BXM 1208	0.248	-2.566	39.168	-85.084	51.090
E-BX 0900	0.188	1.838	0.031	0.235	-2.591
C-LA 2012	1.522	-14.991	57.249	-89.124	48.544

With the tangent shear moduli defined, the stress-logarithmic strain curve from a finite element model of the shear-frame test is compared to the experimental curve to observe the correlation between the model and experiment. Figure A-21 shows the

correlation for the E-LT 5500 biaxial NCF. Because the experimental data are used to obtain the material constants used in the model, the good correlation for the shear-frame data is expected.

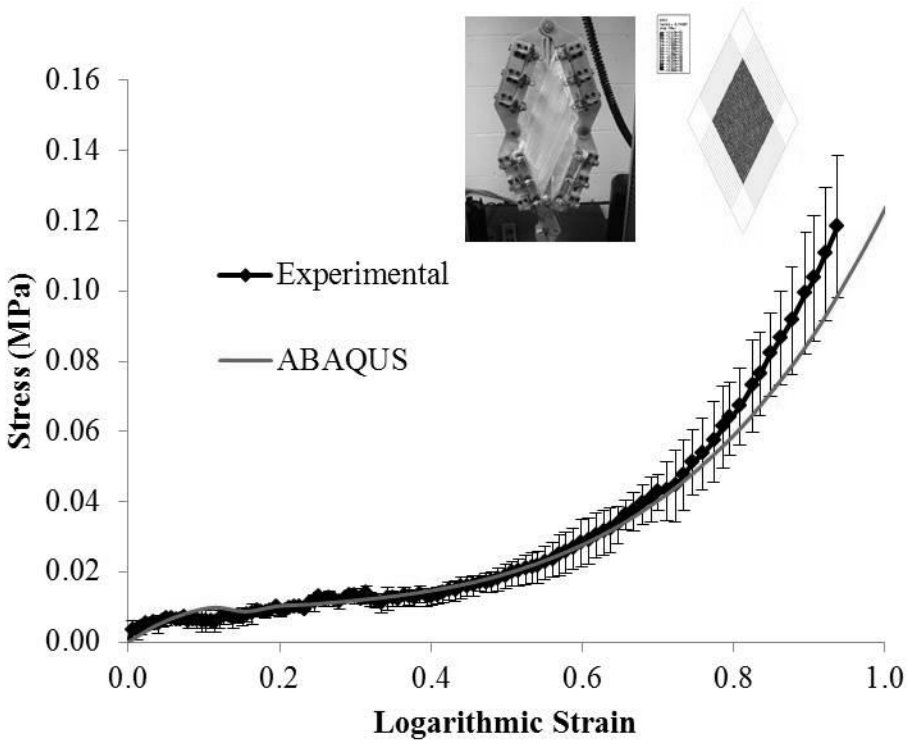

Figure A-21. Shear stress versus logarithmic strain obtained experimentally and from FE model of the shear-frame test for the E-LT 5500 NCF

5.2 TENSILE TEST

To characterize the tensile behavior of a yarn, individual yarns were pulled from the stitched fabric sheets and embedded in tabs, as described in Section 3.2.3, for uniaxial tensile testing. Because the cross-sectional area of the extracted yarns may not necessarily correspond to the manufacturer's definition of the cross-sectional area based on the size and number of fibers bundled together, the linear density [kg/mm] of each

yarn was determined by measuring the mass and the length. This linear density was then divided by the density of the material [kg/mm^3] (Equation 3) to obtain the cross-sectional area.

The measured uniaxial loads were divided by the cross-sectional area of each yarn to determine the tensile stress. Similar to the case of the 2-D shell elements, the VUMAT subroutine requires a tangent modulus, ***D11***, for the 1-D beam elements to define the tensile stiffness. This modulus is essentially the effective elastic modulus of the yarn for that strain, taken from the slope of a linear regression of the experimental stress-true-strain data.

Because all of the fabrics except the carbon unidirectional are made of E-glass material, it was expected that the tensile modulus of the glass fabric yarns would be very similar. Figure A-22 confirms this expectation that the slopes of the stress-true strain curves from several different E-Glass NCFs are similar. Thus, the moduli were averaged and found to be 60.58 GPa, which falls within the range of typical values for E-Glass yarns [12]. For the carbon yarns (C-LA 2012 fabric), the elastic modulus was determined to be 126.65 GPa, which also compares well to typical values [13]. The yarn moduli and their respective cross sectional areas and fracture loads are summarized in Table A-4.

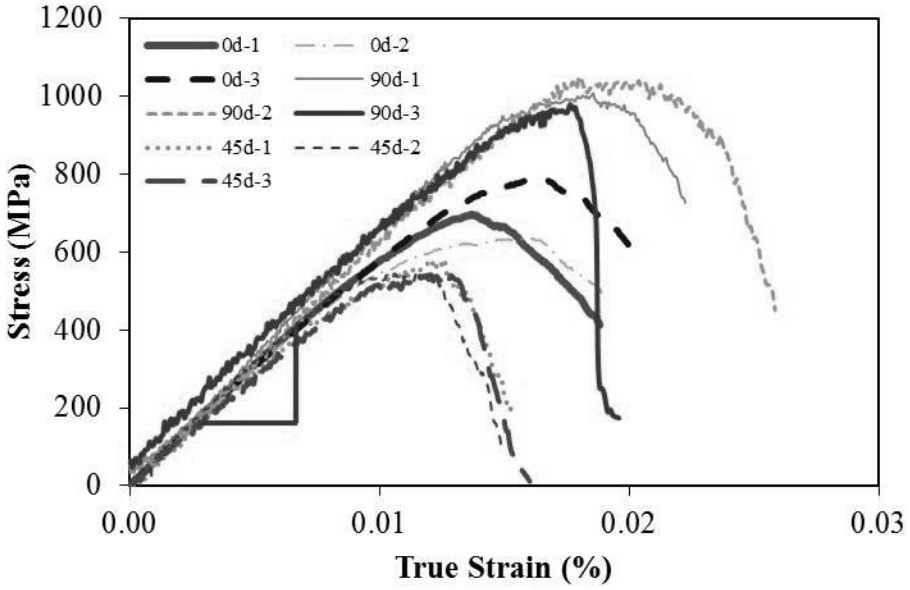

Figure A-22. Stress-true strain curves obtained from uniaxial tensile tests on individual yarns for E-Glass NCFs

Table A-4. Fabric yarn stiffnesses and cross-sectional areas

Fabric	Yarn Orientation (degrees)	Elastic Modulus (GPa)	Cross-sectional Area (mm^2)	Fracture load (N)
E-LT 5500	0	60.58	2.37	1660
	90	60.58	0.22	216
E-LT 2900	0	60.58	1.27	889
	90	60.58	0.22	216
E-BXM 1708	45	60.58	0.13	91
	-45	60.58	0.13	91
E-BXM 1208	45	60.58	0.09	63
	-45	60.58	0.09	63
E-BX 0900	45	60.58	0.16	112
	-45	60.58	0.16	112
C-LA 2012	0	126.65	1.10	1200

Single-yarn FE models comprised of 1-D beam elements were loaded in tension and the resulting stress-true strain curve was plotted (Figure A-23) to check that the tensile modulus, given by the slope of the line, is correctly defined within the VUMAT subroutine.

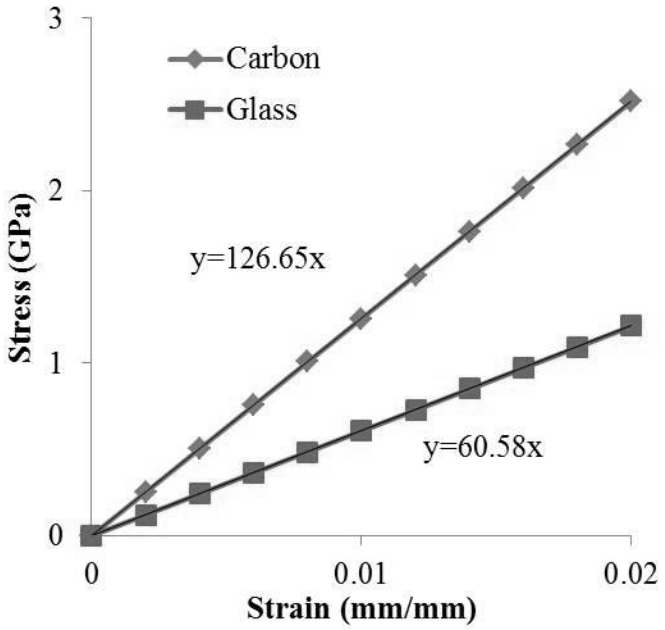

Figure A-23. Tensile stress-strain curves from FE models

5.3 BENDING STIFFNESS TEST

The bending stiffness was measured by hanging a fabric sample and applying a horizontal load to achieve tip displacements of 25.4 mm and 50.8 mm. Two samples of each fabric were tested for repeatability. The total bending stiffness was divided by the number of yarns in the sample to obtain the bending stiffness of each yarn. Likewise, the total load was divided by the number of yarns to obtain the load per yarn necessary for displacing the tip. The 25.4-mm and 50.8-mm tip displacements were then applied to a finite element model of a single yarn and the resulting load per yarn and deformed

profiles were compared to the same parameters measured experimentally using digital images. The coordinates needed to plot the experimental deformed profiles were extracted from the digital images using the software, ImageJ. Figure A-24 shows the measured deformed profile of the E-LT 5500 fabric for the two different tip displacements compared to the deformed profiles of the associated finite element models of the same fabric. The good correlation indicates that the same yarn bending stiffness (400 N-mm^2) defined in the model is capable of capturing the deformed profile and tip load for multiple tip displacements.

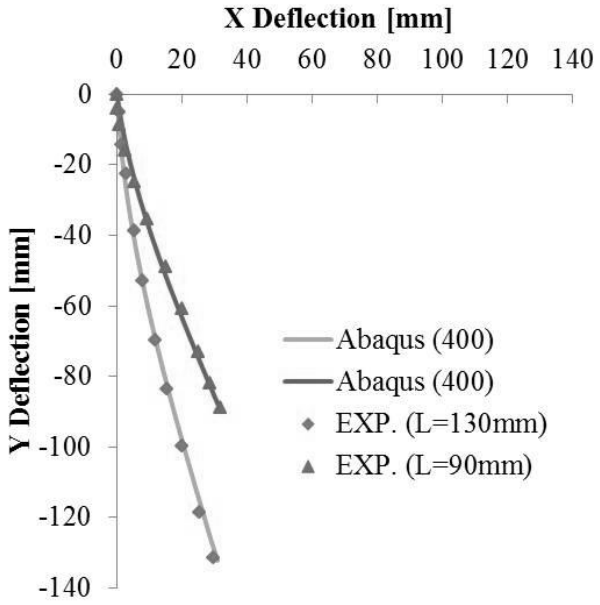

Figure A-24. Comparison of deformed E-LT 5500 fabric profile from bending stiffness test with FE model of the same test at two different tip displacements

The beam section definition in the Abaqus input file must be set to a beam general section with a nonlinear section type. If the default beam section is used and the moment

of inertia is changed to give the equivalent bending stiffness, the fabric model will simply compress into itself rather than buckle (Figure A-25a). The nonlinear section type allows a fabric in compression to buckle out-of-plane (Figure A-25b).

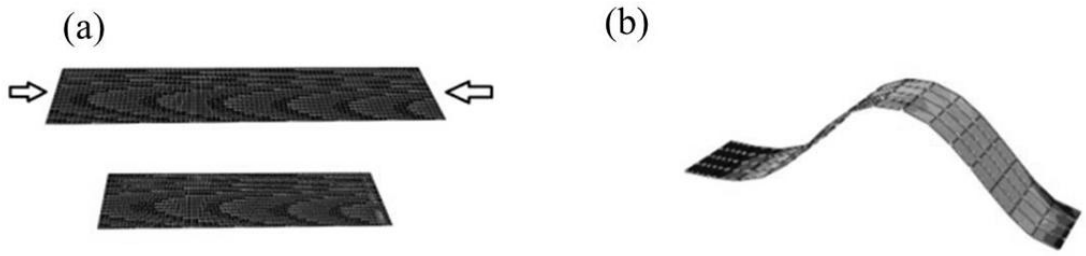

Figure A-25. Finite element compression model using (a) default beam section and (b) nonlinear beam general section

As the preprocessor Abaqus/CAE does not currently support the implementation of the nonlinear section properties, the section properties must be defined manually in the Abaqus input file. The process for determining the bending stiffness of each fabric is iterative. A range of bending-stiffness values is used to replicate the experimental profile shape of the sample. While several values of bending stiffness may lead to a similar profile shape, the force required to displace the tip a known amount is compared to the experimental force to ensure that the correct bending stiffness is being used in the model. Table A-5 summarizes the bending stiffness values determined using this iterative approach.

Table A-5. Bending stiffness values for beam general sections

Fabric	Direction	Bending Stiffness ($N\text{-}mm^2$)
E-LT 5500	**0^o**	400
	90^o	3
E-LT 2900	**0^o**	300
	90^o	3
E-BXM 1708	**$(+)45^o$**	30
	$(-)45^o$	30
E-BXM 1208	**$(+)45^o$**	20
	$(-)45^o$	20
E-BX 0900	**$(+)45^o$**	10
	$(-)45^o$	10
C-LA 2012	**0^o**	300

6 SUMMARY

The mechanical behavior of the NCFs was defined in terms of the in-plane shear stiffness, yarn tensile stiffness and bending stiffness, as well as the friction between contacting layers. A shear-frame test was used to characterize the in-plane shear behavior of each fabric, and uniaxial tensile tests were performed on individual yarns to quantify the tensile stiffness of the fabric yarns. The bending stiffness was characterized by hanging fabric samples vertically and applying a horizontal load to displace the tip of the samples. The deformed profile was plotted digitally and the moment-curvature relation was determined.

LITERATURE CITED

[1] Li, Xiang.: "Material Characterization of Woven-Fabric Composites and Finite Element Analysis of the Thermostamping Process", D.Eng. Dissertation, Dept. of Mechanical Engineering, University of Massachusetts Lowell, 2005.

[2] Jauffrès, D., Sherwood, J.A., Morris, C.D., and Chen, J.: "Discrete mesoscopic modelling for the simulation of woven-fabric reinforcement forming", International Journal of Material Forming, 2009.

[3] Fetfatsidis, K.A., Gamache, L., Sherwood, J.A., Jauffrès, D., and Chen J.: "Design of an apparatus for measuring tool/fabric and fabric/fabric friction of woven-fabric composites during the thermostamping process". International Journal of Material Forming (Accepted for Publication), 2011.

[4] Cao J., Akkerman R., Boisse P., Chen J., Cheng H. S., DeGraaf E. F., Gorczyca J., Harrison P., Hivet G., Launay J., Lee W., Liu L., Lomov S., Long A., Deluycker E., Morestin F., Padvoiskis J., Peng X. Q., Sherwood J., Stoilova T., Tao X. M., Verpoest I., Willems A., Wiggers J., Yu T. X., Zhu B.: Characterization of mechanical behavior of woven fabrics: experimental methods and benchmark results. Composites: Part A, 39:1037-1053, 2008.

[5] Jauffres D., Morris C. D., Sherwood J., Chen J. Simulation of the thermostamping of woven composites: determination of the tensile and in-plane shearing behaviors. 12th ESAFORM Conference. Twente, Nederlands, 2009.

[6] Lomov S., Boisse P., Deluycker E., Morestin F., Vanclooster K., Vandepitte D., Verpoest I., Willems A.: Full-field strain measurements in textile deformability studies. Composites: Part A, 39:1232-1244, 2008.

[7] Petrov, A.S., Sherwood, J.A., Fetfatsidis, K.A.: "Characterization and Finite Element Modeling of Unidirectional Non-Crimp Fabric for Composite Manufacturing", Proceedings of the 15th ESAFORM Conference, Erlangen, Germany, 2012.

[8] Lomov S., Willems A., Verpoest I., Zhu Y., Barburski M., Stoilova T.: Picture frame test of woven composite reinforcements with full-field strain registration. Textile Research Journal, 76:243-252, 2006.

[9] Boisse, P., Hamila, N., Vidal- Sallé, E., Dumont, F.: "Simulation of wrinkling during textile composite reinforcement forming. Influence of tensile, in-plane shear and

bending stiffnesses", *Composites Sci. and Tech.*, 10.1016/j.compscitech.2011.01.011 (2010).

[10] de Bilbao, E., Soulat, D., Hivet, G., and Gasser, A.: Experimental Study of Bending Behaviour of Reinforcements. Experimental Mechanics, March 2009.

[11] Soteropoulos, D., Fetfatsidis, K., Sherwood, J., and Langworthy, J.: "Digital Method of Analyzing the Bending Stiffness of Non-Crimp Fabrics", Proceedings of the 14th ESAFORM Conference, Belfast, United Kingdom, 2011.

[12] The Engineering Toolbox http://www.engineeringtoolbox.com/young-modulus-d_417.html (last checked April 9, 2012)

[13] Performance Composites, Ltd. http://www.performance-composites.com/carbonfibre/mechanicalproperties_2.asp (last checked April 9, 2012)